The Distance-Dependence of Colloidal Au-Amplified Surface Plasmon Resonance

Lin He,*,† Emily A. Smith,‡ Michael J. Natan,§ and Christine D. Keating*

Department of Chemistry, The Pennsylvania State University, University Park, Pennsylvania 16802-6300

Received: April 2, 2004; In Final Form: May 7, 2004

Au nanoparticle-amplified surface plasmon resonance (PA-SPR), like traditional SPR, is typically used to detect binding events at a thin noble metal film. Here we describe the use of SiO_2-overcoated Au films as a substrate for PA-SPR. Changes in SPR angle shift upon Au nanosphere binding were investigated as a function of the SiO_2 thickness. In these experiments, a submonolayer of Au nanoparticles was immobilized atop a thin Au film separated by an intervening SiO_2 layer. Although SPR is an evanescent wave technique, the observed SPR angle shift does not decrease monotonically with increasing Au nanoparticle−Au surface separation, but rather increases to a maximum at ∼32 nm separation before decreasing. In contrast to the previously proposed electromagnetic coupling between the metal particles and the surface as the main cause for the observed distance-dependent SPR response, we propose and have demonstrated qualitatively that the energy modulating capability of the SiO_2 spacing layer is the main contributor. The impact of the particle size, composition, and surface densities on this maximum in SPR angle shifts was also examined. The results indicate that the optimal SiO_2 thickness was independent of Au nanoparticle surface coverage for coverage less than 10%. This work extends the use of PA-SPR to monitoring binding events at glass interfaces and points to a route for increased sensitivity, as evidenced in an PA-SPR assay for human immunoglobin G in a sandwich immunoassay format.

Introduction

Surface plasmon resonance (SPR) has been widely employed for protein−protein interaction studies in which changes in refractive index close to a thin metal surface are monitored.[1−8] The need for significant surface refractive index changes for detection, however, has limited its applications for ultrasensitive bioanalysis. To address this limitation, several signal-amplification approaches have been developed.[9−18] Of those, the use of colloidal Au nanoparticles to enhance SPR signals associated with biochemical binding events has attracted great attention.[18−24] In this method, molecular-recognition probes are pre-conjugated to metallic nanoparticles. The binding events between the probes and their partners on the surface lead to subsequent immobilization of particles on SPR substrates. As a result, remarkably large changes in both the position of the SPR angle and the magnitude of film reflectivity are observed. The successful application of this method has been demonstrated for sandwich immunoassays and DNA hybridization detection by various groups.[11,18,20,23] In addition, the impact of nanoparticle binding on SPR response has been investigated as a function of particle composition, size, surface coverage, and substrate metals.[21,25−29] Metal nanoparticle-modified thin metal films have also been employed as new geometries for prism- and grating-free surface plasmon excitation[30] and in nanoparticle-enhanced thin film photodetectors.[31]

The intensity of surface plasmon propagation, as for any evanescent wave, decays exponentially from the metal−dielectric interface.[32] Thus, a significant reduction in SPR response is expected—and typically observed—as binding events occur farther away from the metal substrate. Indeed, this effect has been used to monitor conformational changes in proteins.[33−35] When the measured response arises from other factors in addition to the evanescent field intensity, more complex distance-dependent phenomena are observed. A classic example is fluorescence emission near metal surfaces. At short distances, the metal surface provides an additional route for nonradiative decay, leading to decreased emission lifetime, while at larger separations enhanced electromagnetic fields can dramatically increase fluorescence efficiency.[36,37] Thus, an optimal metal−fluorophore separation exists at which surface-enhanced emission is observed.[36,37]

It has been postulated that electromagnetic coupling between metal nanoparticles and the thin metal films used as SPR substrates might lead to a similarly complex distance-dependent response.[38] Although evidence of electromagnetic coupling abounds,[30,38−41] literature reports have argued both for[38] and against[40] the presence of a maximum in SPR response at intermediate metal nanoparticle−metal film separations.

Herein, we systematically vary the thickness of an intervening SiO_2 layer between an Au SPR substrate and spherical Au nanoparticles to study this distance-dependent phenomenon, with the aim of addressing the discrepancy observed in the literature. For the system studied, a maximum in angle shifts is observed for intermediate separations, similar to the findings of Holland and Hall.[38] Instead of ascribing the results to electromagnetic coupling between the metal particles and the metal film, however, we demonstrate that the same effect can be observed experimentally and by modeling when the metal particles are replaced by nonmetallic materials. Therefore, we propose that this maximum arises largely due to field modulations caused by the dielectric spacer itself, although minor contribution due

* Corresponding authors. (He) Phone: 1-919-515-2993, E-mail: lin_he@ncsu.edu; Keating. Phone: 1-814-863-7832, E-mail: keating@chem.psu.edu.

† Current address: Department of Chemistry, North Carolina State University, Raleigh, NC 27695.

‡ Current address: Department of Chemistry, University of Arizona, Tucson, AZ 85721.

§ Current address: Nanoplex Technologies, Inc., 1430 O'Brien Drive, Menlo Park, CA 94025.

10.1021/jp048536k CCC: $27.50
Published on Web 07/07/2004

to electromagnetic coupling cannot be ruled out. The impact of particle size, surface coverage, and composition on the particle-amplified (PA)-SPR response are investigated. This work also provides an alternative surface chemistry for downstream chemical derivatization in, for example, biosensing applications. Increased sensitivity for a Au nanoparticle-amplified SPR sandwich immunoassay when performed on this SiO_2-coated Au substrate is demonstrated.

Experimental Section

Materials. Trisodium citrate dihydrate, 3-mercaptoethylamine (MEA), and 3-mercaptopropionic acid (MPA) were obtained from Aldrich. 3-Mercaptopropylmethyldimethoxysilane (MPMDMS) and 3-aminopropyltrimethoxysilane (APTMS) were purchased from United Chemical Technologies. 3-(Triethoxysilyl)propylsuccinic anhydride (TESPSA, 95%) was from Gelest, Inc. $HAuCl_4 \cdot 3H_2O$ was purchased from Acros. Carboxylated polystyrene beads (20 nm diameter) were purchased from Bangs Labs, and diluted to 10% with H_2O before attaching to surfaces. 1-Ethyl-3-(3-dimethylaminopropyl)carbodiimide (EDC), *N*-hydroxysulfosuccinimide (NHS), and goat anti-human immunoglobulin G (α-h-IgG, γ chain specific) were from Pierce. Human immunoglobulin G (h-IgG), goat anti-human immunoglobulin G (α-h-IgG, F_c chain specific), and bovine serum albumin (BSA) were purchased from Sigma. Au (99.99%) and SiO_x (99%) shots used for evaporation were obtained from Johnson-Matthey Corp. Fisher Premium Microscope cover slips (BK7, $n = 1.52$) were used as SPR substrates. All reagents were used as received without further purification. All H_2O (>18 MΩ) used was distilled and then filtered through a Barnstead Nanopure system.

Colloidal Au nanoparticles (12-nm diameters) were prepared by citrate reduction of $HAuCl_4 \cdot 3H_2O$ as previously described.[42,43] Larger diameter colloidal Au (45 nm) was prepared by seeding 12-nm Au with NH_2OH following reported protocols.[44] Average particle diameters were obtained by transmission electron microscopy (TEM) analysis. Optical spectra of colloidal Au solutions were recorded using a HP 8452A spectrophotometer to ensure consistent solution concentrations. A refractive index of bulk Au material in place of Au colloidal particles, $n = 0.173 + 3.422i$, is used for theoretical modeling.

Protein conjugates were prepared following published protocols.[18] Specifically, 60 μg of α-h-IgG (F_c chain specific) was incubated with 1 mL ofcolloidal Au solution (~17 nM) on ice for 1 h. After centrifugation at 12500*g* for 45 min, the supernatant was removed, and the resulting protein/Au conjugates were resuspended in H_2O. Conjugates were used as prepared.

SPR Surface Preparation. Glass substrates were cleaned by sonicating in CH_3OH, CH_3COCH_3, and then CH_3OH for 10 min each. Glass slides were then functionalized by immersion in a 5% MPMDMS/CH_3OH (v/v) solution for 1 h. Thin Au films (48 or 300 nm) were deposited on the silanized surfaces in an Edwards Auto 306 thermal evaporation system. Metal deposition occurred at a pressure of 2×10^{-6} mbar at 0.2 nm/s, monitored by an internal QCM crystal calibrated for Au deposition. Surface roughness was greatly reduced by annealing Au substrates in a home-built oven at 300 °C for 15 min under Ar. After derivatizing Au surface with 5% APTMS/CH_3OH solution for 15 min, various amounts of SiO_x were deposited at 4×10^{-7} mbar and 0.1 nm/s. Deposition of SiO_x onto a 48-nm and a 300-nm Au surface, used for the SPR and ellipsometry measurements, respectively, was performed simultaneously. Certain error in film thickness was expected for deposition of materials other than Au shots; thus ellipsometry and AFM were used to calibrate the actual SiO_2 film thickness. Upon opening the evaporator chamber, the SiO_x film (<50 nm) quickly oxidized in air to SiO_2.[45] Substrates were then stored under Ar in parafilm-sealed containers overnight to prevent any contamination. Prior to colloidal Au immobilization, surfaces were again derivatized with a 5% APTMS/CH_3OH solution for 15 min. Diluted 12-nm colloidal Au solution (1:1 with H_2O, ~8.5 nM) was drop-coated onto the substrates until the desired surface coverage was achieved. Substrates were then rinsed with H_2O and dried under Ar. Colloidal Au particles of 45-nm size were immobilized in the same fashion. Surface density was kept constant for data comparison. To immobilize 20-nm (hydrated diameter) carboxylated polystyrene beads (PS) on the surface, a diluted PS solution was drop-coated on the APTMS-derivatized surface for 30 min to achieve a similar surface coverage, followed by a thorough rinsing. The beads shrank to approximately 10 nm upon drying under Ar, as determined by atomic force microscopy (AFM) (data not shown). A surface density of ~8% was obtained using this method.

SCHEME 1: Distance-Dependent SPR Surface Assembly I

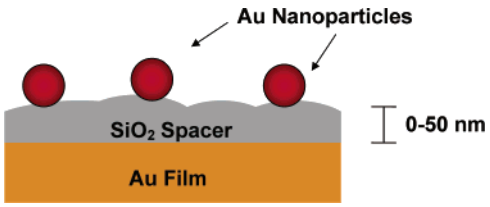

SCHEME 2: Distance-Dependent SPR Surface Assembly II

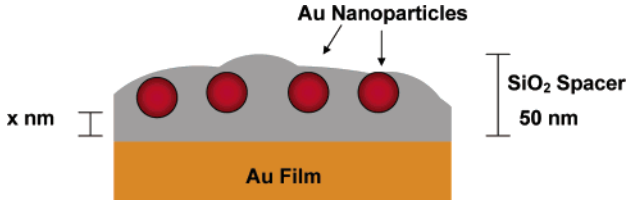

For IgG immunoassay, surfaces were prepared as previously reported.[18] Briefly, bare Au surfaces and 25 nm SiO_2-coated surfaces were derivatized with 10-mM MEA and 5% APTMS for 30 min, respectively. A 1:1 diluted Au colloid solution was applied for varying time periods to achieve the desired surface coverage. In the sandwich immunoassay experiment, a Au surface and a 25 nm SiO_2-coated surface were first derivatized with 10-mM MPA or 5% TESPSA for 30 min. α-h-IgG (γ chain specific) was immobilized on the surfaces through EDC/NHS cross-linking. After rinsing the surface with H_2O and blocking the surface with 10 mg/mL BSA for 15 min, it was incubated with 100 μL of 1 ng/mL h-IgG for 30 min. The surface was then exposed to α-h-IgG (F_c chain specific)/Au conjugate (~15 nM) for detection.

Instrumentation. *Surface Plasmon Resonance (SPR).* A home-built scanning SPR apparatus, as previously described, was used in this work.[18] To minimize errors from slight variations in the thicknesses of films prepared in different batches, a bare Au film that was prepared in the same batch was always measured first as the internal standard. SPR curves were then collected from the SiO_2-coated Au surfaces before and after colloidal Au immobilization. The difference of surface plasmon angles at the minimum SPR reflectivity was calculated, and plotted as a function of film thickness. Each point was an average of three measurements that were taken approximately

2-mm apart on the same surface to minimize the effects of surface heterogeneity.

Ellipsometry. A Rudolph Auto El ellipsometer was used to measure the film thickness of SiO_2-coated substrates with a 300-nm Au film underneath. The measurements were carried out at 70° with an excitation of 632.8 nm (He−Ne laser). The measurements were taken from three different spots on each surface.

Atomic Force Microscopy (AFM). AFM images of samples were measured after SPR measurements. Images were captured in the tapping mode on a Digital Nanoscope IIIa instrument. Two $5 \times 5\ \mu$m images were collected for each surface to ensure a homogeneous coverage, and three $1 \times 1\ \mu$m images were collected for calculating surface coverage by manually counting particles. AFM was also used to double-check the thickness of the SiO_2 layers. By carefully scratching the surface with the blunt end of a pair of tweezers, the thickness of the spacing layer was determined by measuring the abrupt height change at the edge of the scratch.

Modeling. Fresnel equation-based modeling was conducted for the system in which Au nanoparticles were immobilized atop SiO_2 layers. The program used, N-phase SPRangle, was generously provided by Prof. R. Corn (U. Wisconsin). Simple 4-phase modeling programs are available on the Corn group website, and the N-phase program was acquired by submitting a request through the website.[46] Due to the low particle densities (3.4% or 8%) used throughout our experiments, the Maxwell−Garnett equation was used to estimate the average refractive index of Au attached layers.[19,47] A continuous protein layer in the place of the Au nanoparticle layer was used for the modeling of nondipole analyte attachment. The SPR angles obtained from the modeling[48] at various SiO_2 spacer thicknesses (SiO_2 = 0−100 nm) were subtracted with the SPR angle at $SiO_2 = 0$ nm. The differences, i.e., SPR angle shifts, were plotted as a function of SiO_2 thicknesses to compare with the experimental results.

Results and Discussion

Dependence of PA-SPR on Particle−Surface Separation. We have experimentally investigated the effect of particle−surface separation distance upon PA-SPR response for the experimental system depicted in Scheme 1. A SiO_2 spacer layer was placed between a Au thin film SPR substrate and a submonolayer of monodisperse 12-nm diameter Au nanospheres. The thickness of the SiO_2 spacer was varied to investigate the distance-dependence of the Au nanosphere−Au film interaction. SiO_2 was used as the spacing material here for its transparency, rigidity, and ease of preparation.[45] It is also a very common substrate for biological assays, and has been shown to give very low nonspecific nanoparticle binding in other types of Au nanobioconjugate-based bioassays.[49] SiO_2 film thickness was monitored by QCM during vapor deposition and verified after deposition using ellipsometry and AFM (Supporting Information). Au nanospheres are chosen in PA-SPR for its high optical density. It also enables greater control over nanoparticle size, shape, and surface coverage than has been previously employed in distance-dependence studies, which relied on vapor deposited or sputtered Ag nanoparticles.[38−41]

The self-assembly of Au nanoparticle submonolayers on organosilane-coated glass surfaces has been well-documented in the literature.[50] This chemistry was adapted to affix Au colloids atop SiO_2-coated surfaces via electrostatic interactions between aminated silanes on the SiO_2 and the negatively charged Au nanoparticles. On the basis of the known kinetics and thermodynamics of colloidal Au immobilization, a series of samples was prepared with desired particle coverage (Supporting Information).[51,52] For most of the experiments described here, a coverage of 3×10^{10} particles/cm^2 was used, corresponding to 3.4% monolayer coverage. Three AFM images of these surfaces were used for coverage measurements. Any substrate with more than 10% variation in particle density was discarded. Therefore, in further discussions, we will assume that contributions to SPR angle shifts from variations in Au nanoparticle coverage are negligible unless specified.

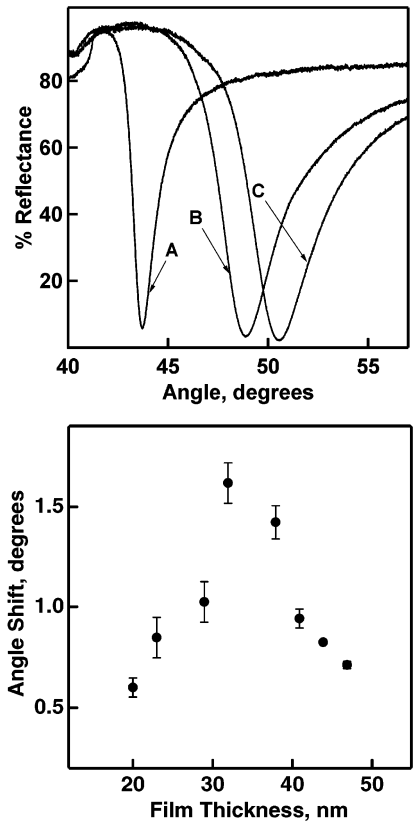

Figure 1. (Top) SPR curves obtained from a bare Au film (A), SiO_2-coated surface without (B) or with (C) colloidal Au particles attached. The angle shift referred in the text was calculated as the surface plasmon angle difference between the minimums of curve B and C. (Bottom) The SPR angle shifts before and after 12-nm colloidal Au immobilization as a function of the particle/surface distance. Surface coverage is ~3.4%. The error bars are calculated as standard deviations of three measurements.

The top panel of Figure 1 shows representative SPR curves collected from a bare Au substrate and from a SiO_2-coated surface before and after Au nanoparticle immobilization (curves A, B, and C, respectively). A pronounced SPR angle shift is observed at each coating step. In addition, a significant increase in curve width and a slight change in the surface reflectance at the SPR angle occur. All three parameters—the angle of minimum reflectivity, the width of the SPR curve, and the absolute reflectance—are related to the plasmon propagation on the surface. For simplicity, the shift in angle of minimum reflectivity was chosen to correlate the particle−surface separation with the changes in SPR response. The difference between the plasmon resonance angles in curve B and C (i.e., the shift associated with Au nanoparticle binding) is referred to here as the SPR angle shift (ΔSPR), and is plotted as a function of the separation between Au colloidal particles and the SPR substrate.

The magnitude of SPR angle shift increased initially as particle−surface separation was increased (Figure 1, bottom). After reaching a maximum (d_{max}) where Au colloidal particles

were placed approximately 32 ± 5 nm away from the surface, a decrease in SPR response was apparent. The error bars in this panel are the standard deviation of three different measurements from each sample, taken approximately 2-mm apart to minimize the effects of surface heterogeneity. Increased surface roughness from SiO_2 deposition and the Au particle attachment led to a significantly decreased SPR curve quality, resulting in the large error bars observed. Note that the EM field distribution is most sensitive to the roughness near the metal substrate, thus the scattering due to surface irregularity at the SiO_2/air interface decreases upon larger separation. As a result, the error in the measurement is significantly reduced for the substrates with thicker SiO_2 coatings (Figure 1, bottom).

Discussion of PA-SPR Distance-Dependence. Two groups have previously investigated the separation-dependence of SPR for metal nanoparticle-modified films.[38−41] Both studies stressed the importance of coupling between the localized surface plasmon resonance (LSPR) of metallic particles and the surface plasmon propagation (SPP) of the metal film underneath; however, their results were quite different. Holland and Hall observed an optimal thickness of LiF spacer layer between a Ag film and a Ag island nanoparticulate layer.[38] In contrast, Kume et al. found only a decrease in coupling with increasing thickness of an SiO_2 spacer between an Al film and a sputtered Ag nanoparticle/SiO_2 composite layer.[40]

Both the experimental geometry (Scheme 1) and the observed separation corresponding to maximum SPR response in our experiment for the Au nanoparticle−SiO_2 Au film system ($d_{max} \approx 32$ nm) (Figure 1, bottom) is similar to that reported by Holland and Hall for the Ag island−LiF−Ag system ($d_{max} = 25$ nm).[38] These authors investigated several excitation wavelengths, and observed a maximum in SPR shift as a function of separation at every wavelength. As expected, the distance-dependent phenomenon was more pronounced at wavelengths closer to the LSPR of the Ag nanoparticles (~400 nm), which supports the notion of the presence of the electromagnetic coupling between metallic nanoparticles and the metal surface nearby.[38,39] However, the effects of other possible factors, i.e., surface-roughness-caused light scattering, energy modulation by the dielectric layer, were not discussed.

Independently, Kume et al. used a different sample setup to reduce radiative energy dissipation (scattering) from the particle-induced surface roughness. These samples differed from those of Holland and Hall, beyond the Al substrate, in that the total thickness of SiO_2 was held constant, with the Ag nanoparticles incorporated at different heights within the SiO_2 film by a co-sputtering process.[40] Thus, the Ag nanoparticles were *embedded within* a SiO_2 layer, while in the Holland and Hall experiments nanoparticles were *placed atop* a dielectric layer. This geometry reduced the light scattering caused by the increased surface roughness upon particle attachment. The wavelength-dependence of both SPR angle shift[40] and light emission from the film due to scattering by the nanoparticles[41] again indicate significant electromagnetic coupling between the Al film and the particles. Interestingly, this coupling was maximized at zero separation, and dropped off with increasing separation, unlike the Holland and Hall results.[38] Note that the separations investigated by Kume et al. were 0, 18, and 24 nm; given the nanoparticle diameter (~4 nm) and the relatively low coverage (5%) in these experiments, it is possible that an optimum separation occurred below 18 nm, and could have been missed in the experiment.

To examine this speculation, we repeated our experiments, this time embedding the Au nanospheres at different depths in the SiO_2 (Scheme 2). The total thickness of the SiO_2/Au particle layer was held constant at 50 nm. Figure 2 compares results for the geometries shown in Schemes 1 and 2. In contrast to what has been reported by Kume et al., embedding the Au nanoparticles within the SiO_2 layer still resulted in larger angle shifts overall, indicating that factors other than the exponential decay of the EM field intensity controlled the SPR response.

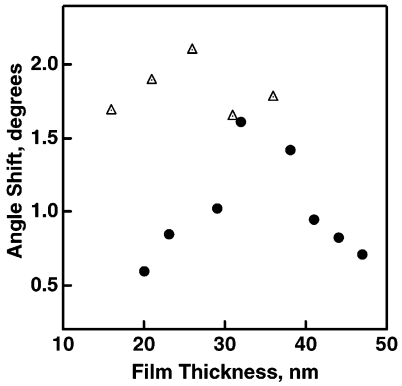

Figure 2. The SPR angle shifts as functions of the particle/surface distance. 12-nm colloidal Au was immobilized atop (●) or embedded in (△) the SiO_2 layer.

It has been reported that an additional layer of dielectric leads to an increased field intensity at the dielectric−air interface by modulating the electromagnetic field energy redistribution among different layers.[53−58] Specifically, a thin layer of high dielectric material atop the metallic surface alters the energy distribution in the metal, dielectric, and sensing layers, resulting in an increase in electric field intensity just outside the dielectric spacer (i.e., at the spacer−air interface where sensing is to occur). This effect has been demonstrated for ZrO_2 layers atop Ag films by van Gent and co-workers, who found good agreement between experiment and simulation.[53] Dielectric layers have been used previously to increase the dynamic range of SPR sensors.[59,60]

To dissect the contributions from the SiO_2 spacer from those of electromagnetic coupling between the metallic nanoparticles and the Au film, we replaced the Au particles with nonmetallic (polystyrene) nanoparticles of the same size and at the same surface coverage.[61] Any distance-dependence observed in this experiment indicates mechanisms not unique to metallic nanoparticles (i.e., not electromagnetic coupling). An increase in SPR shift, albeit less pronounced, was clearly observed as polystyrene−Au substrate separation increased; these data support the attribution of the initial distance-dependence to the increasing thickness of the SiO_2 spacing layer, rather than exclusively to electromagnetic coupling between the particles and the metal film (Figure 3, top, Δ). The magnitude of the increase in the SPR response for polystyrene bead attachment is much smaller than that observed from Au particle-coated surfaces of the same coverage, a result more of the lower optical density of polystyrene beads than the possible presence of the electromagnetic coupling. The importance of the spacing layer is also supported by a theoretical calculation in which a 5-layer system (prism−Au film−SiO_2 layer−protein layer−air, Figure 3, bottom) with SiO_2 of different thickness is modeled using the Fresnel equation.[48] A similar dependence of SPR shift for Au colloidal particle−absorbed surface with increased layer−metal film separation was also modeled (Figure 3, bottom, inset). Both results confirm the important role of SiO_2 spacers in modulating the energy field intensity, disregarding the nature, nonmetallic or metallic, of the absorbed layer. The much smaller angle shifts observed are not unexpected in the calculated results, given the Fresnel equation being based on perfectly smooth interfaces in

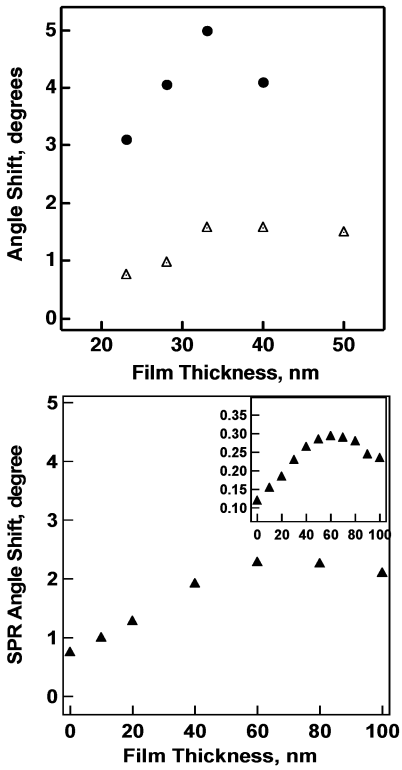

Figure 3. Comparison of metallic and nonmetallic nanoparticle (8% surface coverage) on the distance-dependent SPR response. (Top) 12-nm colloidal Au (●) or polystyrene beads (△) were immobilized on the top of SiO_2 spacer. (Bottom) Theoretical modeling of a protein layer (▲) atop of SiO_2 spacer. The insert shows the theoretical modeling of 12 nm Au colloidal particles absorbed on SiO_2 surface at 8%.

the thin film stack. In reality, colloidal particles (Au or polystyrene) act as localized defects or roughness sites on the metal surface, and greatly affect surface morphology,[24,40,41,62,63] as evidenced by the pronounced SPR curve broadening and depth changes characteristic of PA-SPR (Figure 1, top, curve C).[23−27]

Light scattering due to the presence of metallic particles and the roughened surface (reduced in Kume's experiments) also plays a role in the observed distance-dependent SPR phenomenon. Particle-mediated scattering can be seen in our data as the broadening of the SPR curves, and has been directly monitored by several groups as emission from the SPR film.[31,38,40,41]

Reexamination of the results published by Holland and Hall for the Ag/LiF/Ag island nanoparticle system[38,39] and by Kume for the Al/SiO_2 with embedded Ag nanoparticles[40] shows that these previous reports are also consistent with the interpretation proposed here. Specifically, when metal particles are separated from a planar metal film by a dielectric of variable thickness, an optimum separation is observed. This can be explained as an initial increase due to compression of the evanescent electromagnetic field inside or outside of the dielectric layer, followed ultimately by a decrease as the dielectric becomes quite thick and the field compression is insufficient to compensate for the decrease in EM field intensity reaching the far side of the dielectric.

Effect of Au Nanosphere Size and Spacing. We have investigated Au nanosphere size and spacing effect to confirm the nominal contribution of EM coupling in our systems. Any electromagnetic coupling between metal particles and the Au film is expected to be strongly dependent upon nanoparticle diameter and spacing; previous work *without* a dielectric spacer has demonstrated dramatically increased angle shifts for higher coverage nanoparticle films as well as larger diameter particles.[19,25] In our experiments, an improved SPR response was observed at a somewhat higher coverage (~8% as compared to 3.4% coverage in Figure 1), a result of the increased volume fraction of Au colloid on the surface (Figure 4, top). Note that even at this surface density, interparticle coupling was not strong enough to change d_{max} since most particles were still far apart from each other.[64−66] As the particle density was further increased, a shift of the optimal distance to a larger value would be expected from increased EM coupling (long-range SP coupling) between the neighboring particles. It is noted that the underlying Au film may play a role in interparticle coupling at small separation distances, extending the length scales over which the nanoparticles can interact; strong coupling has been demonstrated for larger Au structures on Au films lacking a dielectric spacer.[67] However, this effect is expected to be relatively small for the experimental geometry used here.

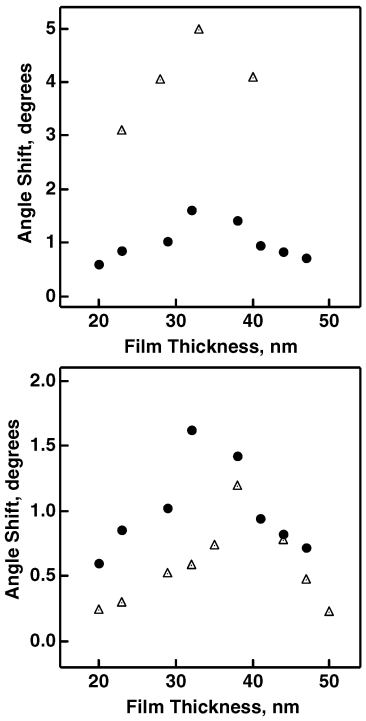

Figure 4. (Top) Effect of particle coverage on the distance-dependent SPR response. The surface coverage of 12-nm diameter Au nanoparticles is 8% (△) and 3.4% (●). (Bottom) Effect of particle size on the distance-dependent SPR response. 12-nm (●) or 45-nm (△) colloidal Au was immobilized on the surface with the same volume fraction.

The distance response curve observed for 45-nm diameter particles was similar to that for 12-nm particles; however, the separation corresponding to maximum angle shift was increased for the larger diameter particles (Figure 4, bottom). In this experiment, surface coverage was chosen to hold the surface volume fraction constant. While a surface coverage of 20 particles/μm^2 (calc. 3.2% surface coverage) used in the experiment is too dilute to cause any significant particle coupling,[68] the optimal separation is still shifted to a larger position (Figure 4, bottom). We believe that the increased SP coupling between particles and the surface and/or the presence of particle clusters result in the change of d_{max}.[58,69−72]

Summary of the Distance-Dependent PA-SPR Effect

In summary, we propose here that the presence of a maximum in SPR response as particle−surface separation increases is

SCHEME 3: Sandwich Immunoassay via Distance-Amplified Au−SPR

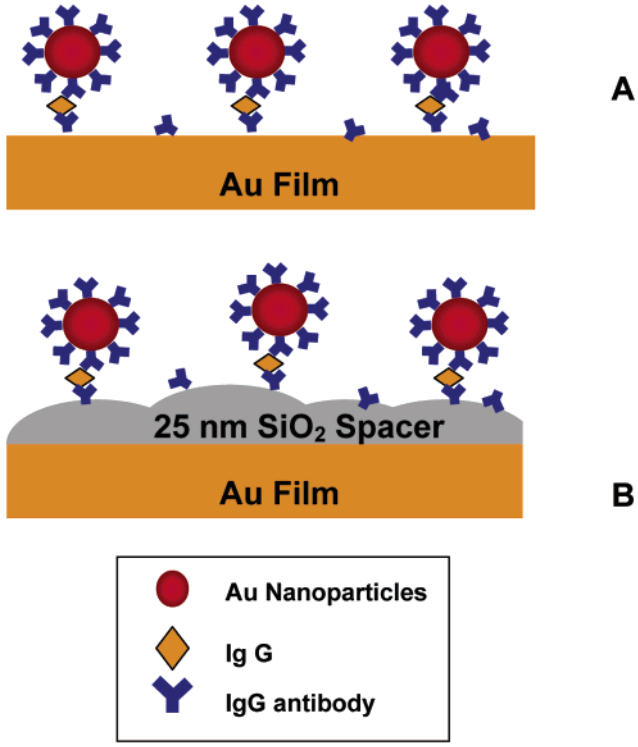

mainly due to the modulated field intensity by the SiO_2 overlayer. This finding is supported by our experimental results and the theoretical modeling. When the impact of the dielectric is taken into consideration, the differences in Holland and Hall's and Kume's results are not unexpected, nor are the differences in our two experimental geometries (particles on top of SiO_2 vs particles embedded in SiO_2). The existence of electromagnetic interactions between the metallic nanoparticles and the surface, and light scattering are also thought to play some role. Especially for relatively small separations and large particles, some electromagnetic coupling between the surface and the metallic nanoparticles is expected. While quantification of the contribution from each factor was not possible in the current work, our results highlight the importance of the dielectric of the spacer layer in dictating the d_{max}.

PA-SPR Sandwich Immunoassay on SiO_2-Modified Film. Coating the SPR surface with an additional dielectric layer can be beneficial in several regards: different derivatization chemistries can be adapted for SiO_2-coated surfaces for the immobilization of biomolecules; thus further expanding the applicability of SPR beyond the reflective metals typically employed. In addition, the nonspecific particle adsorption of biomolecules on a noble metal surface, which limited the sensitivity of PA-SPR based bioassays,[23] may be reduced using a glass-coated surface. An inert SiO_2 coating may also provide short-term protection for metal surfaces that are easily oxidized (e.g., Ag), opening up opportunities for using metal substrates of optimal optical properties in SPR studies. As shown in the results presented here, this additional layer also provides an interesting route to further improve the sensitivity of Au-amplified SPR by detecting chemical events at a certain distance above the surface.

An immunochemical assay was carried out to demonstrate the feasibility of distance-amplified SPR for protein detection (Scheme 3). As shown in Figure 5, 1 ng/mL of h-IgG (~6.7 pM) was detected with an angle shift of 0.26° using Au-

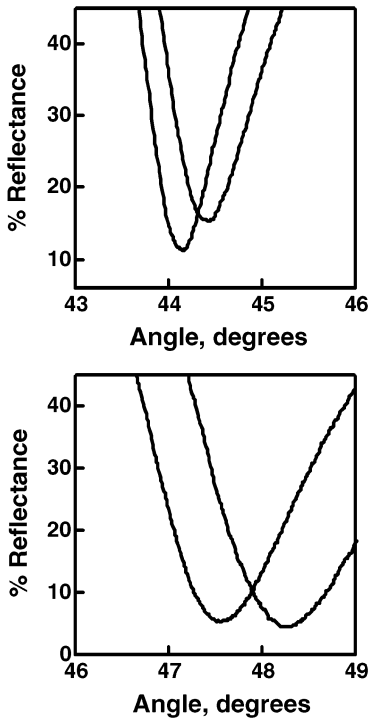

Figure 5. In-situ SPR curves of an evaporated Au film modified with α-h-IgG (γ chain specific), followed with exposure to 1 ng/mL h-IgG (left curve), and α-h-IgG (Fc specific)/Au conjugates (right curve) on bare Au surface (top panel) and 25-nm SiO_2-coated Au surface (bottom panel).

amplified SPR on a bare Au surface (top), while a much larger angle shift (0.85°) was observed from 25-nm SiO_2-coated surface (bottom). These results demonstrated that the intervening glass layer does not preclude the use of SPR for biomolecular binding studies. Although the SiO_2-coated surface gave a broader curve as compared with the uncoated surface, it also resulted in a 3-fold enhancement in SPR angle shift. This increase in sensitivity comes on top of the 1000-fold increases in sensitivity reported for Au nanoparticle-amplified SPR without the intervening SiO_2 layer.[23] The SPR shift for a given SiO_2 thickness is roughly linear with Au nanoparticle coverage (Supporting Information), and therefore may be useful in bioassay quantification. Note that the expected SPR angle shift upon Au−protein conjugates immobilization can only be obtained through a standard assay titration, as it critically depends on the increased film thickness after the primary antibody and antigen bindings, the final surface density of Au−protein conjugates, and the size of Au−protein conjugates. It is also noted that the increased calibration slope and the limited useful range of angles that can be scanned will inevitably limit the dynamic range of the technique. Nevertheless, it is expected that the potential of extending PA-SPR to a wide variety of previously inaccessible interfacial systems with an increase in sensitivity will, in many cases, outweigh this limitation.

Conclusion

In conclusion, a distance-dependent SPR response was observed and a correlation of SPR angle shift-vs-separation distance was established for the Au thin film−SiO_2 overlayer−Au nanoparticle system. Our results for the first time point to the importance of field modulation by the dielectric spacer layer in the distance-dependent PA-SPR response. The existence of the optimal distance in the SPR dispersion curve allows further sensitivity improvement in Au-amplified SPR by

detecting chemical events at certain positions away from the metallic surface. The same concept is also amenable to use in imaging SPR experiments.

We note that the Au nanoparticle system used here offers a greater degree of control over particle size, shape, and surface coverage as compared to previous studies employing sputtered or vapor-deposited Ag nanoparticles. Thus, this system may also be useful for future comparisons of experimental and theoretical results for coupling between nanoparticle localized surface plasmon (LSPR) and surface plasmon polariton (SPP) in thin metal films.

Acknowledgment. The authors acknowledge Prof. R. Corn and the Corn research group for generously providing the N-phase Fresnel calculation program, and the National Institutes of Health for support of this research (R01 EB000268, R01 GM55312, R21 HG02102).

Supporting Information Available: Comparison of film thickness measured by ellipsometry and AFM, AFM images of particle coverage on SiO_2-coated surfaces, and SPR angle shift calibration on different surfaces (3 pages). This material is available free of charge via the Internet at http://pubs.acs.org.

References and Notes

(1) (a) Wegner, G. J.; Lee, H. J.; Marriott, G.; Corn, R. M. *Anal. Chem.* **2003**, *75*, 4740−4746. (b) Goodrich, T. T.; Lee, H. J.; Corn, R. M. *J. Am. Chem. Soc.* **2004**, *126*, 4086−4087.

(2) Shumaker-Parry, J. S.; Zareie, M. H.; Aebersold, R.; Campbell, C. T. *Anal. Chem.* **2004**, *76*, 918−929.

(3) Praig, V. G.; Hall, E. A. H. *Anal. Chim. Acta* **2003**, *500*, 323−336.

(4) Lofas, S. *Mod. Drug Discovery* **2003**, *6*, 47−49.

(5) Mozsolits, H.; Aguilar, M.-I. *Biopolymers* **2002**, *66*, 3−18.

(6) Homola, J.; Yee, S. S.; Myszka, D. In *Optical Biosensors: Present and Future*; Ligler, F. S. R. T., Ed.; Elsevier: Amsterdam, 2002; pp 207−251.

(7) van der Merwe, P. A.; Harding, N. S. E.; Chowdhry, B. Z. *Protein−Ligand Interactions: Hydrodynamics and Calorimetry*; Oxford University Press: Oxford, 2001; pp 137−170.

(8) McDonnell, J. M. *Curr. Opin. Chem. Biol.* **2001**, *5*, 572−577.

(9) Wink, T.; van Zuilen, S. J.; Bult, A.; van Bennekom, W. P. *Anal. Chem.* **1998**, *70*, 827−832.

(10) Yamaguchi, H.; Harada, A. *Chem. Lett.* **2002**, *3*, 382−383.

(11) Zhao, H. Q.; Lin, L.; Li, J. R.; Tang, J. A.; Duan, M. X.; Jiang, L. *J. Nanopart. Res.* **2001**, *3*, 321−323.

(12) Pei, R. J.; Yang, X. R.; Wang, E. K. *Analyst* **2001**, *126*, 4−6.

(13) Pei, R. J.; Yang, X. R.; Wang, E. K. *Anal. Chim. Acta* **2002**, *453*, 173−179.

(14) Devries, E. F. A.; Schasfoort, R. B. M.; Vanderplas, J.; Greve, J. *Biosens. Bioelectron.* **1994**, *9*, 509−514.

(15) Kricka, L. J. *Clin. Chem.* **1994**, *40*, 347−357.

(16) Sato, Y.; Ikegaki, S.; Suzuki, K.; Kawaguchi, H. *J. Biomater. Sci., Polym.* **2003**, *14*, 803−820.

(17) Yamaguchi, Y.; Harada, A. *Biomacromolecules* **2002**, *3*, 1163−1169.

(18) Lyon, L. A.; Musick, M. D.; Natan, M. J. *Anal. Chem.* **1998**, *70*, 5177−5183.

(19) Leung, P.-T.; Pollard-Knight, D.; Malan, G. P.; Finlan, M. F. *Sens. Actuators, B* **1994**, *22*, 175−180.

(20) Yamaguchi, A.; Juodkazis, S.; Matsuo, S.; Misawa, H. *Chem. Lett.* **2002**, *2*, 190−191.

(21) Hutter, E.; Chah, S.; Liu, J. F.; Park, J.; Yi, J. Fendler, J. H.; Roy, D. *J. Phys. Chem. B* **2001**, *105*, 8−12.

(22) Riboh, J. C.; Haes, A. J.; McFarland, A. D.; Yonzon, C. R. van Duyne, R. P. *J. Phys. Chem. B* **2003**, *107*, 1772−1780.

(23) He, L.; Musick, M. D.; Nicewarner, S. R.; Salinas, F. G.; Benkovic, S. J.; Natan, M. J.; Keating, C. D. *J. Am. Chem. Soc.* **2000**, *122*, 9071−9077.

(24) Natan, M. J.; Lyon, L. A. In *Metal Nanoparticles*; Feldheim, D. L., Foss, C. A., Jr., Eds.; Marcel Dekker: New York, 2002; pp 183−205.

(25) Lyon, L. A.; Pena, D. J.; Natan, M. J. *J. Phys. Chem. B* **1999**, *103*, 5826−5831.

(26) Lyon, L. A.; Holliway, W. D.; Natan, M. J. *Rev. Sci. Instrum.* **1999**, *70*, 2076−2081.

(27) Lyon, L. A.; Musick, M. D.; Smith, P. C.; Reiss, B. D.; Pena, D. J.; Natan, M. J. *Sens. Actuator B−Chem.* **1999**, *54*, 118−124.

(28) Hutter, E.; Fendler, J. H.; Roy, D. *J. Phys. Chem. B* **2001**, *105*, 11159−11168.

(29) Chah, S.; Hutter, E.; Roy, D.; Fendler, J. H.; Yi, J. *Chem. Phys.* **2001**, *272*, 127−136.

(30) Hayashi, S.; Kume, T.; Amano, T.; Yamamoto, K. *Jpn. J. Appl. Phys.* **1996**, *35*, L331-L334.

(31) Stuart, H. R.; Hall, D. G. *Appl. Phys. Lett.* **1996**, *69*, 2327−2329.

(32) Ekgasit, S.; Thammacharoen, C.; Yu, F.; Knoll, W. *Anal. Chem.* **2004**, *76*, 2210−2219.

(33) (a) Stenlund, P.; Babcock, G. J.; Sodroski, J.; Myszka, D. G. *Anal. Biochem.* **2003**, *316*, 243−250. (b) Paynter, S.; Russell, D. A. *Anal. Biochem.* **2002**, *309*, 85−89.

(34) Gestwicki, J. E.; Hsieh, H. V.; Pitner, J. B. *Anal. Chem.* **2001**, *73*, 5732−5737.

(35) Chah, S.; Kumar, C. V.; Hammond, M. R.; Zare, R. N. *Anal. Chem.* **2004**, *76*, 2112−2117.

(36) (a) Moskovits, M. *Rev. Mod. Phys.* **1985**, *57*, 783−826. (b) Neumann, T.; Johansson, M.-L.; Kambhampati, D.; Knoll, W. *Adv. Funct. Mater.* **2002**, *12*, 575−586. (c) Pockrand, I.; Brillante, A.; Mobius, D. *Chem. Phys. Lett.* **1980**, *69*, 499−504.

(37) (a) Wokaun, A.; Lutz, H.-P.; King, A. P.; Wild, U. P.; Ernst, R. R. *J. Chem. Phys.* **1983**, *79*, 509−514. (b) Kummerlen, J.; Leitner, A.; Brunner, H.; Aussenegg, F. R.; Wokaun, A. *Mol. Phys.* **1993**, *80*, 1031−1046. (c) Kittredge, K.; Fox, M. A.; Whitesell, J. K. J. *Phys. Chem. B* **2001**, *105*, 10594−10599. (d) Tarcha, P. J.; DeSaja-Gonzalez, J.; Rodriguez-Llorente, S.; Aroca, R. *Appl. Spectrosc.* **1999**, *53*, 43−48. (e) Sokolov, K.; Chumanov, G.; Cotton, T. M. *Anal. Chem.* **1998**, *70*, 3898−3905.

(38) Holland, W. R.; Hall, D. G. *Phys. Rev. B* **1983**, *27*, 7765−7768.

(39) Holland, W. R.; Hall, D. G. *Phys. Rev. Lett.* **1984**, *52*, 1041−1044.

(40) Kume, T.; Nakagawa, N.; Hayashi, S.; Yamamoto, K. *Solid State Commun.* **1995**, *93*, 171−175.

(41) (a) Kume, T.; Hayashi, S.; Yamamoto, K. *Phys. Rev. B* **1997**, *55*, 4774−4782. (b) Hayashi, S.; Kume, T.; Amano, T.; Yamamoto, K. *Jpn. J. Appl. Phys.* **1996**, *35*, L331−L334.

(42) Hayat, M. A. *Colloidal Gold: Principles, Methods, and Applications*; Academic Press: San Diego, 1989.

(43) Grabar, K. C.; Smith, P. C.; Musick, M. D.; Davis, J. A.; Walter, D. G.; Jackson, M. A.; Guthrie, A. P. Natan, M. J. *J. Am. Chem. Soc.* **1996**, *118*, 1148−1153.

(44) (a) Brown, K. R.; Walter, D. G.; Natan, M. J. *Chem. Mater.* **2000**, *12*, 306−313. (b) Brown, K. R.; Natan, M. J. *Langmuir* **1998**, *14*, 726−728.

(45) Ravindra, N. M.; Narayan, J. *J. Appl. Phys.* **1986**, *60*, 1139−1146.

(46) Corn, R. Group Webpage: http://corninfo.chem.wisc.edu/calculations.html. The program is copyrighted by the University of Wisconsin 1998. This web site was supported in part by NSF under Grant 0133151.

(47) Maxwell−Garnett, J. C. *Philos. Trans. R. Soc. London* **1904**, *203*, 385−420.

(48) A 5-layer Fresnel modeling was conducted in which: 1: prism, refractive index of 1.515; 2: Au film 0.173+3.442i, 48 nm; 3: SiO_2 film 1.46, 0−100 nm; 4: air 1.0 or protein 1.5 or Au colloid particles of 1.026 + 0.039i, 6 or 12 nm for protein or Au particles, respectively; 5: air, 1.0.

(49) (a) Taton, T. A.; Mirkin, C. A.; Letsinger, R. L. *Science* **2000**, *289*, 1757−1760. (b) Taton, T. A.; Lu, G.;. Mirkin, C. A. *J. Am. Chem. Soc.* **2001**, *123*, 5164−5165.

(50) (a) Freeman, R. G.; Grabar, K. C.; Allison, K. J.; Bright, R. M.; Davis, J. A.; Guthrie, A. P.; Hommer, M. B.; Jackson, M. A.; Smith, P. C.; Natan, M. J. *Science* **1995**, *267*, 1629−1632. (b) Grabar, K. C.; Freeman, R. G.; Hommer, M. B.; Natan, M. J. *Anal. Chem.* **1995**, *67*, 735−743. (c) Grabar, K. C.; Allison, K. J.; Baker, B. E.; Bright, R. M.; Brown, K. R.; Freeman, R. G.; Fox, A. P.; Keating, C. D.; Musick, M. D.; Natan, M. J. *Langmuir* **1996**, *12*, 2353−2361.

(51) Keating, C. D.; Musick, M. D.; Keefe, M. H.; Natan, M. J. *J. Chem. Educ.* **1999**, *76*, 949−955.

(52) Keating, C. D. Ph.D. Thesis, The Pennsylvania State University, 1997.

(53) van Gent, J.; Lambeck, P. V.; Kreuwel, H. J. M.; Gerritsma, G. J.; Sudholter, E. J. R.; Reinhoudt, D. N.; Popma, T. J. A. *Appl. Opt.* **1990**, *29*, 2843−2849.

(54) Kreuwel, H. J. M. Ph.D. Thesis, University of Twente, Enschede, The Netherlands, 1988.

(55) Pockrand, I. *Surf. Sci.* **1978**, *72*, 577−588.

(56) Negm, S.; Talaat, H. *Solid State Commun.* **1992**, *84*, 133−137.

(57) Patskovsky, S.; Kabashin, A. V.; Meunier, M.; Luong, J. H. T. *Appl. Opt.* **2003**, *42*, 6905−6909.

(58) Tseng, S. M.; Zhan, J.-H. *Jpn. J. Appl. Phys.* **1998**, *37*, L441−L443.

(59) Jorgenson, R. C.; Yee, S. S. *Sens. Act. B* **1994**, *43*, 44−48.

(60) Garces, I.; Aldea, C.; Mateo, J. *Sens. Act. B* **1992**, *7*, 771−774.

(61) Raether, H. *Surface Plasmons on Smooth and Rough Surfaces and on Gratings*; Springer-Verlag: Berlin, New York, 1988.

(62) The refractive index of polystyrene beads is 1.58 + 0.0005i. Ma, X.; Lu, J. Q.; Brock, R. S.; Jacobs, K. M.; Yang, P.; Hu, X.-H. *Phys. Med. Biol.* **2003**, *48*, 4165−4172.

(63) (a) Johansson, P. *Phys. Rev. B* **2001**, *64*, 165405/1−15. (b) Sterligov, V. A.; Chessac, P.; Lysenko, S. I.; Kofman, R. *Opt. Commun.* **2000**, *186*, 27−33. (c) Xiao, M.; Zayats, A.; Siqueiros, J. *Phys. Rev. B* **1997**, *55*, 1824−1837. (d) Jory, M. J.; Cann, P. S.; Sambles, J. R.; Perkins, E. A. *Appl. Phys. Lett.* **2003**, *83*, 3006−3008.

(64) At the "high" surface densities (8%, ∼700 particles/μm^2), the calculated interparticle distance was slightly larger than 3× particle diameter.

(65) Zhao, L.; Kelly, K. L.; Schatz, G. C. *J. Phys. Chem. B* **2003**, *107*, 7343−7350.

(66) Haes, A. J.; Zou, S.; Schatz, G. C.; Van Duyne, R. P. *J. Phys. Chem. B* **2004**, *108*, 109−116.

(67) Felidj, N.; Aubard, J.; Levi, G.; Krenn, J. R.; Schider, G.; Leitner, A.; Aussenegg. F. R. *Phys. Rev. B* **2002**, *66*, 1−7.

(68) In this experiment, the total volume fraction of Au colloid was kept constant to minimize the interference caused from varying the volume fraction of Au attached on the surfaces. A lower surface coverage (∼20 particles/μm^2) was used for 45-nm colloidal Au-attached surface, whereas 300 particles/μm^2 for 12-nm colloidal Au-coated surface.

(69) Hecht, B.; Bielefeldt, H.; Novotny, L.; Inouye, Y.; Pohl, D. W. *Phys. Rev. Lett.* **1996**, *77*, 1889−1892.

(70) Agassi, D. *Phys. Rev. B* **1986**, *33*, 3873−3884.

(71) Simon, H. J.; Guha, J. K. *Opt. Commun.* **1976**, *18*, 391−394.

(72) Rendell, R. W.; Scalapino, D. J.; Muhlschlegel, B. *Phys. Rev. Lett.* **1978**, *41*, 1746−1750.